Editors' Suggestion

Nonresonant Local Fields Enhance Second-Harmonic Generation from Metal Nanoislands with Dielectric Cover

Semyon Chervinskii,[1,2,*] Kalle Koskinen,[3] Sergey Scherbak,[1,4] Martti Kauranen,[3] and Andrey Lipovskii[1,4]
[1]Institute of Physics, Nanotechnology and Telecommunication, Peter the Great St. Petersburg Polytechnic University, Polytechnicheskaya 29, St. Petersburg, 195251 Russia
[2]Institute of Photonics, University of Eastern Finland, P.O. Box 111, FI-80101 Joensuu, Finland
[3]Laboratory of Photonics, Tampere University of Technology, P.O. Box 692, FI-33101 Tampere, Finland
[4]Department of Physics and Technology of Nanostructures, St. Petersburg Academic University, Khlopina 8/3, St. Petersburg, 194021 Russia

(Received 13 October 2017; published 15 March 2018)

We study second-harmonic generation from gold nanoislands covered with amorphous titanium oxide (TiO_2) films. As the TiO_2 thickness increases, the plasmon resonance of the nanoislands shifts away from the second-harmonic wavelength of 532 nm, diminishing the resonant enhancement of the process at this wavelength. Nevertheless, the second-harmonic signal is enhanced by up to a factor of 45 with increasing TiO_2 thickness. This unexpected effect arises from the scaling of local fields at the fundamental wavelength of 1064 nm—which is at the far tail of the resonance—due to a change in the dielectric environment of the nanoislands.

DOI: 10.1103/PhysRevLett.120.113902

The optical properties of metal nanoparticles arise from their localized surface-plasmon resonances (LSPRs). Such resonances give rise to strongly enhanced local fields (LFs) near the metal-dielectric interfaces, advantageous, e.g., for catalytic activity [1], optical absorption and emission [2,3], or Raman scattering [4]. The enhancement is particularly interesting for nonlinear optical processes, which scale with a high power of the optical field [5]. For the particular case of second-harmonic generation (SHG), several studies have addressed plasmon resonances at the fundamental [6,7] and second-harmonic [8–11] wavelengths as well as their interplay with symmetry rules and local-field distributions [8,12–17].

The spectral positions of LSPRs depend on the dielectric environment of the metal particles, which forms the basis for plasmonic sensors [18]. When the particles are covered with a dielectric film of increasing thickness, the spectrum shifts gradually and saturates only when the evanescent tails of the LFs are fully embedded in the dielectric. This can be qualitatively understood by treating thin dielectric films as bulk media with reduced effective permittivity, which grows with the film thickness until the bulk value is reached. The associated spectral shift occurs in parallel with growing particle polarizability and, respectively, the LF at the resonant frequency. Far less known is that the modified LFs are not limited to plasmon resonances. In fact, the dielectric loading increases the particle polarizability, thereby scaling the LFs even when the wavelength is far from the plasmon resonance, providing unexplored opportunities for nanophotonics.

In this Letter, we demonstrate the usefulness of such nonresonant LFs in nonlinear optics. More specifically, we use SHG with the fundamental wavelength of 1064 nm to investigate gold nanoisland films with plasmon resonance at about 520 nm. This is close to the second-harmonic (SH) wavelength of 532 nm, and the process is, therefore, resonantly enhanced at the SH but not at the fundamental wavelength. We then use atomic layer deposition (ALD) to cover the nanoislands with amorphous titanium dioxide (TiO_2) films of increasing thickness. This shifts the plasmon resonance away from the SH wavelength, thereby decreasing the resonance enhancement. Nevertheless, the SH signal from coated nanoislands increases by a factor of 45 with the TiO_2 thickness, while TiO_2 films on silica without nanoislands do not exhibit any remarkable nonlinearity. The increase is well explained by the scaling of the LFs at the fundamental wavelength associated with the increased dielectric loading due to the TiO_2 film.

Our gold nanoisland films were prepared by air annealing of gold films deposited onto fused silica substrates by evaporation. The resulting films were comprised of separate nanoislands of 10–20 nm in size (Fig. 1 inset) [19]. The details related to the preparation of the samples and measurements are presented in the Supplemental Material [20]. The nanoisland films were coated with TiO_2 films of varying thickness (about 3–100 nm) by ALD. Ellipsometric analysis of similar TiO_2 films on substrates without nanoislands showed that their refractive indices varied by about 10% depending on film thickness, probably due to densification of the thickest film in the long

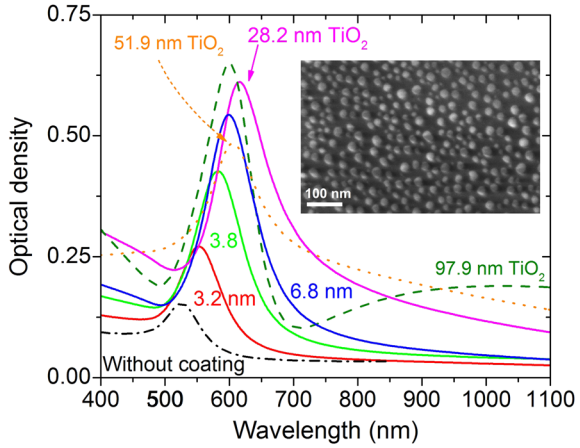

FIG. 1. Absorption spectra of the samples with gold nanoisland film coated with TiO_2 layers of different thicknesses (indicated near the curves). The spectra of the 51.9 and 97.9 nm samples, which demonstrate irregularities, are dotted and dashed, respectively. Inset: SEM image of the nanoisland film.

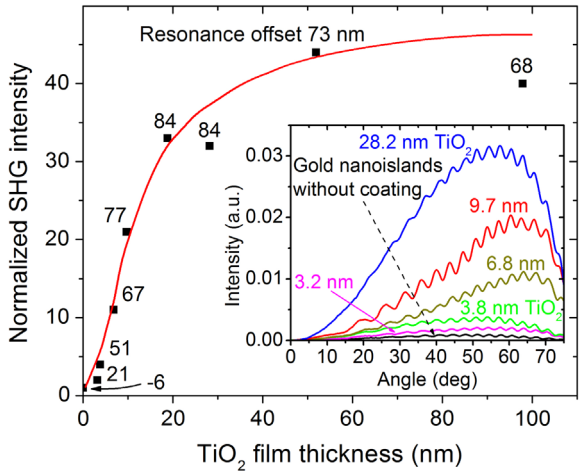

FIG. 2. SH response from gold nanoisland films coated with TiO_2 layers as a function of the TiO_2 layer thickness. The resonance offsets $\Delta\lambda$ (nm) between the LSPR and SH wavelength are indicated near the corresponding data markers. The SH intensity is normalized by the SH signal from the nanoisland film without the TiO_2 cover. The line is a guide for the eye only. Inset: SHG Maker-fringe patterns from representative samples.

ALD process. These differences have no influence on the main results of our work.

The optical spectra of the nanoisland films covered with TiO_2 layers of different thicknesses (Fig. 1) show that the LSPR peak shifts toward longer wavelengths, as known for covered nanoparticles [24–26]. Additionally, the peak becomes more intense with increasing TiO_2 thickness. Both trends saturate after the thickness of about 30 nm when the electric field of the plasmon is completely inside the covering layer [19]. The peak growth is similar to that of metal nanoparticles when they are embedded in more polarizable media [23,27], and this behavior is theoretically well understood [28]. For the two samples with TiO_2 thickness exceeding 30 nm (51.9 and 97.9 nm), the spectra exhibit some irregularities compared to the monotonic trend for thinner TiO_2 films. We relate these irregularities to the very long ALD times of the thickest covers, which could influence the size of the gold nanoislands, and interference effects within the thickest TiO_2 films. Nevertheless, even in these cases, saturation of both the spectral shift and the absorption peak is evident.

The SHG responses of bare TiO_2 films and TiO_2-covered gold nanoisland samples with different TiO_2 thicknesses were characterized using the Maker-fringe technique [29]. A laser with 70 ps pulses at 1064 nm was used as the source of fundamental light [20,30]. Both the fundamental and SH beams were p polarized, which typically gives rise to the strongest SH signals. The experiments result in interference fringes between the SH signals from the sample and the back surface of the substrate as the incident angle is varied, as detailed in the Supplemental Material [20]. Representative Maker fringes from our samples are shown in the Fig. 2 inset, where the SH response increases by a factor of 45 with increasing TiO_2 thickness. We emphasize that the SH signals from bare TiO_2 films of any thickness were about the same and comparable to the signal from the silica substrate, approximately 80 times weaker than the signal from gold nanoislands with no TiO_2 coating. This proves that the TiO_2 films are amorphous as expected from ALD [31].

The dependence of SHG from gold nanoisland films on TiO_2 thickness is shown in Fig. 2. The signal is normalized to that from the nanoisland film without cover. The SH signal saturates at about 30 nm film thickness, near the range where the LSPR spectral shift saturates [19]. Importantly, the SH response grows with the TiO_2 thickness despite the detuning $\Delta\lambda = \lambda_{\mathrm{LSPR}} - 532$ nm of the LSPR wavelength from the SH wavelength (532 nm); see the magnitudes of the resonance offset indicated near the data markers in Fig. 2. A small decrease in the SH signal for the thickest TiO_2 cover is probably related to the effect of the temperature on the gold nanoparticles in the long ALD process.

Physical insight into the observed effects can be obtained by considering the polarizability of a spherical particle of radius R [32],

$$\alpha = R^3 \frac{\varepsilon_{\mathrm{me}} - \varepsilon_{\mathrm{out}}}{\varepsilon_{\mathrm{me}} + 2\varepsilon_{\mathrm{out}}} = R^3 \frac{(\varepsilon_{\mathrm{me}} + 2\varepsilon_{\mathrm{out}}) - 3\varepsilon_{\mathrm{out}}}{\varepsilon_{\mathrm{me}} + 2\varepsilon_{\mathrm{out}}}, \qquad (1)$$

where $\varepsilon_{\mathrm{me}}$ is the permittivity for the metal and $\varepsilon_{\mathrm{out}}$ that for the embedding medium. By assuming that $\varepsilon_{\mathrm{out}}$ is real and by separating $\varepsilon_{\mathrm{me}}$ into its real and imaginary parts $\varepsilon_{\mathrm{me}} = \varepsilon'_{\mathrm{me}} + i\varepsilon''_{\mathrm{me}}$, it is evident that the polarizability exhibits a resonance when $\varepsilon'_{\mathrm{me}} = -2\varepsilon_{\mathrm{out}}$. The absorption cross section of the particles, which is of interest here, depends on the imaginary part of the polarizability

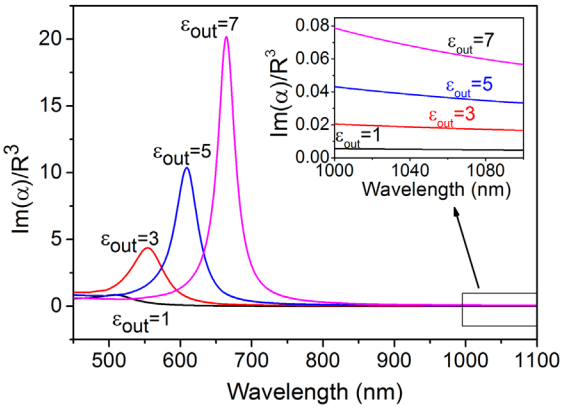

FIG. 3. Influence of outer medium permittivity (ε_{out}) on the dispersion of the imaginary part of the polarizability of a spherical gold nanoparticle of radius R.

$[\sigma^{\text{abs}} \propto \text{Im}(\alpha)]$ [33]. The imaginary part of the resonant polarizability is, thus,

$$\text{Im}(\alpha_{\text{res}}) = 3R^3 \frac{\varepsilon_{\text{out}}}{\varepsilon''_{\text{me}}}; \tag{2}$$

i.e., it is proportional to the permittivity of the outer medium. The real part ε'_{me} for metals becomes more negative with increasing wavelength. By then treating the layer of the embedding medium by effective permittivity, which increases with film thickness, it becomes clear that the resonance shifts to longer wavelengths and becomes more intense as the layer thickness increases. Note that the imaginary part $\varepsilon''_{\text{me}}$ for metals is assumed to be small, which allowed neglecting the real part of the resonant polarizability.

It is less evident, however, that this thickness-dependent scaling is not limited to the line center of LSPR. Equation (1) typically leads to a Lorentzian line shape. If its linewidth does not change much with the thickness of the outer medium, the tails of the LSPR must increase in the same proportion as at the line center. We applied this simple model for small gold spheres using the Johnson-Christy data [34] for the permittivity of gold. The results are illustrated in Fig. 3 for the imaginary part of the polarizability. When the effective permittivity is increased, the resonance shifts and becomes more intense, as observed experimentally (Fig. 1). Furthermore, the increase also affects the tails of the LSPR, reaching the fundamental wavelength of the laser. Finally, similar effects occur also for the real part of the polarizability. The changes in the LFs arise from both the real and imaginary parts of the polarizability and are, therefore, fully carried through to the tails of the resonance.

For a more detailed treatment of the observed effects, we need both the linear polarizability of the gold nanoparticles and the local-field factors (LFFs) near the particles. For this, we use an approach [19,35] where the polarizability and corresponding electric potential of a truncated

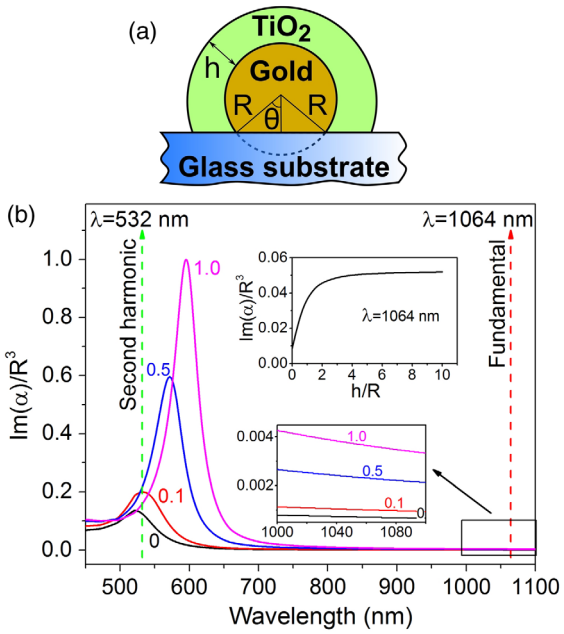

FIG. 4. (a) Schematic of a truncated gold nanosphere on a glass substrate and covered with a TiO_2 layer, θ-truncation angle. (b) Influence of the TiO_2 ($\varepsilon_{\text{coat}} = 5.5$) cover of different thickness (h) on the imaginary part of the polarizability of a truncated gold sphere (truncation angle ~50°) of radius R placed on a substrate with $\varepsilon_{\text{sub}} = 2.25$; the h/R ratio is labeled near the curves. Inset: Polarizability at the fundamental wavelength 1064 nm vs the h/R ratio. Dispersions of the substrate and the cover are neglected.

nanosphere on a substrate [see Fig. 4(a)] are calculated in quasistatic approximation. In the following, we present the results for the case where the field is polarized along the glass surface. The normal polarization components are known to exhibit similar behavior albeit scaled by a factor that depends on the truncation angle [36].

We applied this model to small gold nanoparticles with radius R by using the Johnson-Christy data for the permittivity of gold [34]. The truncation angle was taken to be $\theta = 50°$ [Fig. 4(a)]. The permittivity of TiO_2 was taken to be $\varepsilon_{\text{coat}} = 5.5$ and its thickness h was varied. The permittivity of the glass substrate was taken to be $\varepsilon_{\text{sub}} = 2.25$. The absorption spectrum [Fig. 4(b)] is seen to depend on the ratio h/R.

The general behavior again follows that of the absorption presented in Fig. 1. The LSPR is seen to shift toward longer wavelengths and become more intense with increasing cover thickness. The shift has been discussed elsewhere [19,37], while not much attention has been paid to the growth in polarizability [38]. A key difference between the experiments and simulations is that the latter exhibit higher LSPR quality factors. This is because the simulations did not account for deviations in the size and shape of the particles in the real samples or for the mutual interaction between the particles. The trend in the polarizability is similar to the one for spherical particles in a medium with

effective polarizability (Fig. 3). The polarizability at our fundamental wavelength, i.e., the far tail of the LSPR, grows rapidly with the TiO_2 cover thickness and starts saturating at the ratio h/R of about 3 [inset of Fig. 4(b)]. For our nanoisland samples with average radius of ~9 nm, this corresponds to ~30 nm thick TiO_2 cover, in very good agreement with the experiment (Fig. 1 inset).

We next apply this model to interpret our experimental results for SHG. For this, we need the LFFs at the fundamental and SH wavelengths. For nanoparticles, the LFFs are space dependent, describing the redistribution of optical energy to "hot spots," and tensorial, because the LFs can contain polarization components not present in the incident field. Keeping these limitations in mind, the source polarization for SHG can be written as [39]

$$P_{2\omega} = \chi^{(2)}_{\text{eff}} L_{2\omega} L^2_{\omega} E^2_{0\omega}, \tag{3}$$

where $\chi^{(2)}_{\text{eff}}$ is the effective second-order susceptibility, L_ω and $L_{2\omega}$ are the LFFs at the fundamental and SH frequencies, respectively, and $E_{0\omega}$ is the incident field at the fundamental frequency. Thus, the SHG intensity depends on the LFFs as

$$I_{\text{SHG}} \propto L^2_{2\omega} L^4_{\omega}. \tag{4}$$

It is crucial that the dependence at the fundamental frequency is to the fourth power and at the SH frequency, it is to the second power.

The application of Eqs. (3) and (4) depends greatly on how the effective susceptibility $\chi^{(2)}_{\text{eff}}$ is chosen. We assume that the SH response arises from the surface nonlinearity of the gold particles and that the dominant tensor component of the surface susceptibility is $\chi^{(2)}_{S,\perp\perp\perp}$, where $\perp$ refers to the normal component, as justified in a number of works [40–42]. This local response, thus, needs to be integrated over the shape of the nanoparticle. Therefore, the LFF for frequency Ω is defined as

$$L^{\perp}_{\Omega} = \frac{\langle |E^{\perp}_{\Omega}(r = R)| \rangle_{\theta,\phi}}{|E^0_{\Omega}|}, \tag{5}$$

where E^0_Ω is the incident electric field, $E^{\perp}_{\Omega}(r = R)$ the local normal component of the field on the particle surface, and $\langle \cdots \rangle_{\theta,\phi}$ denotes angular averaging, with θ and ϕ being spherical coordinates for the truncated nanosphere.

The SH intensity calculated according to Eq. (4) as a function of dielectric coating thickness h for truncated gold nanoparticles of radius R is shown in Fig. 5, while the powers of calculated LFFs L_ω and $L_{2\omega}$ [Eq. (3)] are presented in the inset.

The expected resonant behavior of the LFF at the SHG frequency $L_{2\omega}$ is evident in the inset in Fig. 5. The LSPR passes through the SH wavelength ($\lambda = 532$ nm) for very thin coatings, but this resonance is quickly lost as the coating thickness increases. The fundamental wavelength ($\lambda = 1064$ nm), on the other hand, is at the far tail of the LSPR, and the LFF L_ω monotonically grows with the coating thickness. Obviously, these differences are accentuated for the higher powers of the LFFs. The average particle radius in our case is about 9 nm [19], so the h/R ratio for the maximum cover thickness of 100 nm is about 11. All the LFFs for SHG [Eq. (4)] are combined in Fig. 5. The contribution of the monotonic growth of L_ω is seen to override any resonant features of $L_{2\omega}$. This, of course, arises because the scaling with L_ω is to the fourth power, whereas with $L_{2\omega}$, it is only to the second power.

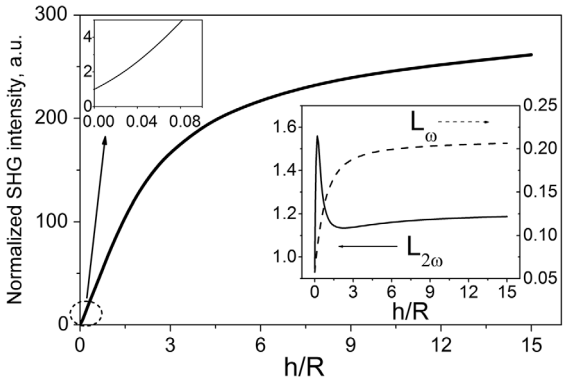

FIG. 5. Calculated SH intensity for truncated spherical gold nanoparticles (50° truncation angle) on a glass surface ($\varepsilon_{\text{sub}} = 2.25$) as a function of the TiO_2 ($\varepsilon_{\text{coat}} = 5.5$) coating thickness. The intensity is normalized by the SH signal from bare gold nanoparticles ($h = 0$). Inset: Calculated LFFs at the fundamental and SH frequencies. Dispersions of the substrate and the cover are neglected.

The qualitative agreement for the SH signal strength between the experimental results (Fig. 2) and theory (Fig. 5) is seen to be very good. The main difference is that the experimental enhancement is about a factor of 45, whereas the theory predicts a factor of 240 for $h/R = 11$. The factor of 5 discrepancy in SH intensity, however, corresponds to only a factor of 1.5 difference in field amplitude. This difference can be, for example, due to the size distribution of the nanoparticles and due to Fresnel reflections at the air-TiO_2 interfaces, which could be remedied by antireflection coatings on the interfaces.

Our results have links to nonlinear composite materials [43,44]. The focus in that area has been on bulk-type composite materials with different dielectric properties. In addition, the role of a host material with high permittivity on enhancing nonlinear properties has been emphasized [45]. On the other hand, for metal-dielectric composites, only the role of plasmon resonances is usually considered [46–49]. The present work goes beyond these earlier results by highlighting how systematic variations in the dielectric environment affect the nonlinear responses and how the local-field effects at nonresonant wavelengths can completely overrule the role of any resonant effects.

It is evident that the theoretical analysis of the present results can be significantly improved. In particular, we describe the local nonlinearity of the metal-dielectric interface by a single component of the susceptibility tensor. By more extensive modeling, additional components could be included, as has been done for nonlinear scattering [42,50] and numerical description of nonlinear metamaterials [41]. A more important future question, however, is to consider how the local-field effects influence the overall response of our samples. It is likely that due to the anisotropy of our thin-film structure, the local-field effects are different for different polarization components of the fundamental and SH beams. Such effect would then influence different tensor components of the sample in different ways, whereas the present results were discussed only in terms of an effective scalar SH susceptibility. However, such additional factors have no influence on the main results of the present Letter.

In conclusion, we showed that covering metal nanoparticles with a dielectric coating allows the efficiency of second-harmonic generation to be enhanced, independent of the spectral position of the localized surface-plasmon resonance of the particles. The enhancement was observed for gold nanoislands covered with a dielectric layer of amorphous titanium dioxide of varying thickness. We modeled and explained this phenomenon by the growth of the local-field factors at the fundamental wavelength. This growth dominates the decrease in the local-field factors at the second-harmonic wavelength caused by the shift of the plasmon resonance away from the second-harmonic wavelength. The importance of the LFFs at the fundamental wavelength over those at the second-harmonic wavelength arises because the second-harmonic signal is proportional to the second power of the local-field factors at the second-harmonic wavelength and to the fourth power of those at the fundamental wavelength. We believe that this phenomenon is of great importance and can be observed in a variety of contexts, independent of the particular shape or even size of the nanoparticles. In addition, the effect is not limited to second-harmonic generation but should open new opportunities in all cases where the tailoring of the local fields can be used to advantage in photonic applications.

The authors are grateful to Igor Reduto for SEM measurements. S. Ch. is thankful to Niko Penttinen and Pertti Pääkkönen for the introduction to ellipsometry. The study has been supported by Academy of Finland (Grants No. 287651 and No. 309473) and the Russian Ministry for Education and Science Project No. 3.2869.2017. K. K. acknowledges the Vilho, Yrjö, and Kalle Väisälä Foundation for a personal fellowship.

S. Ch., K. K., and S. Sch. contributed equally to this work.

*Corresponding author.
semen.chervinskii@uef.fi

[1] E. C. Le Ru and P. G. Etchegoin, *Principles of Surface-Enhanced Raman Spectroscopy* (Elsevier Science, New York, 2009).
[2] V. A. Podolskiy, P. Ginzburg, B. Wells, and A. V. Zayats, Faraday Discuss. **178**, 61 (2015)
[3] M. A. Green and S. Pillai, Nat. Photonics **6**, 130 (2012).
[4] J. N. Anker, W. P. Hall, O. Lyandres, N. C. Shah, J. Zhao, and R. P. Van Duyne, Nat. Mater. **7**, 442 (2008).
[5] M. Kauranen and A. V. Zayats, Nat. Photonics **6**, 737 (2012).
[6] R. Czaplicki, M. Zdanowicz, K. Koskinen, J. Laukkanen, M. Kuittinen, and M. Kauranen, Opt. Express **19**, 26866 (2011).
[7] F. B. P. Niesler, N. Feth, S. Linden, and M. Wegener, Opt. Lett. **36**, 1533 (2011).
[8] K. Thyagarajan, S. Rivier, A. Lovera, and O. J. F. Martin, Opt. Express **20**, 12860 (2012).
[9] M. Celebrano, X. Wu, M. Baselli, S. Großmann, P. Biagioni, A. Locatelli, C. de Angelis, G. Cerullo, R. Osellame, B. Hecht, L. Duò, F. Ciccacci, and M. Finazzi, Nat. Nanotechnol. **10**, 412 (2015).
[10] B. Metzger, L. Gui, J. Fuchs, D. Floess, M. Hentschel, and H. Giessen, Nano Lett. **15**, 3917 (2015).
[11] H. Linnenbank and S. Linden, Optica **2**, 698 (2015).
[12] B. K. Canfield, H. Husu, J. Laukkanen, B. F. Bai, M. Kuittinen, J. Turunen, and M. Kauranen, Nano Lett. **7**, 1251 (2007).
[13] J. Berthelot, G. Bachelier, M. Song, P. Rai, G. Colas des Francs, A. Dereux, and A. Bouhelier, Opt. Express **20**, 10498 (2012).
[14] R. Czaplicki, J. Mäkitalo, R. Siikanen, H. Husu, J. Lehtolahti, M. Kuittinen, and M. Kauranen, Nano Lett. **15**, 530 (2015).
[15] S. D. Gennaro, M. Rahmani, V. Giannini, H. Aouani, T. P. H. Sidiropoulos, M. Navarro-Cía, S. A. Maier, and R. F. Oulton, Nano Lett. **16**, 5278 (2016).
[16] S. Viarbitskaya, O. Demichel, B. Cluzel, G. Colas des Francs, and A. Bouhelier, Phys. Rev. Lett. **115**, 197401 (2015).
[17] F. Wang, A. B. F. Martinson, and H. Harutyunyan, ACS Photonics **4**, 1188 (2017).
[18] M. Li, S. K. Cushing, and N. Q. Wu, Analyst **140**, 386 (2015).
[19] S. Scherbak, N. Kapralov, I. Reduto, S. Chervinskii, O. Svirko, and A. A. Lipovskii, Plasmonics **12**, 1903 (2017).
[20] See Supplemental Material at http://link.aps.org/supplemental/10.1103/PhysRevLett.120.113902 which includes Refs. [21–23] for details of the samples preparation and measurements.
[21] B. von Blanckenhagen, D. Tonova, and J. Ullmann, Appl. Opt. **41**, 3137 (2002).
[22] G. E. Jellison and F. A. Modine, Appl. Phys. Lett. **69**, 371 (1996).
[23] H. X. Xu and M. Kall, Sens. Actuators B **87**, 244 (2002).
[24] P. Royer, J. P. Goudonnet, R. J. Warmack, and T. L. Ferrell, Phys. Rev. B **35**, 3753 (1987).

[25] W. Ji-Fei, L. Hong-Jian, Z. Zi-You, L. Xue-Yong, L. Ju, and Y. Hai-Yan, Chin. Phys. B **19**, 117310 (2010).
[26] J. A. Dieringer, A. D. McFarland, N. C. Shah, D. A. Stuart, A. V. Whitney, C. R. Yonzon, M. A. Young, X. Zhang, and R. P. Van Duyne, Faraday Discuss. **132**, 9 (2006).
[27] T. Okamoto, I. Yamaguchi, and T. Kobayashi, Opt. Lett. **25**, 372 (2000).
[28] V. Klimov, *Nanoplasmonics* (CRC Press, Boca Raton, 2013).
[29] P. D. Maker, R. W. Terhune, M. Nisenhoff, and C. M. Savage, Phys. Rev. Lett. **8**, 21 (1962).
[30] T. Ning, H. Pietarinen, O. Hyvärinen, J. Simonen, G. Genty, and M. Kauranen, Appl. Phys. Lett. **100**, 161902 (2012).
[31] M. R. Saleem, S. Honkanen, and J. Turunen, Appl. Opt. **52**, 422 (2013).
[32] J. D. Jackson, *Classical Electrodynamics*, 3rd ed. (John Wiley & Sons Inc., New York, 1999).
[33] C. F. Bohren and D. R. Huffman, *Absorption and Scattering of Light by Small Particles* (John Wiley & Sons Inc., New York, 1983).
[34] P. Johnson and R. Christy, Phys. Rev. B **6**, 4370 (1972).
[35] M. M. Wind, J. Vlieger, and D. Bedeaux, Physica (Amsterdam) **141A**, 33 (1987).
[36] M. M. Wind, J. Vlieger, and D. Bedeaux, Physica (Amsterdam) **143A**, 164 (1987).
[37] S. Chervinskii, A. Matikainen, A. Dergachev, A. Lipovskii, and S. Honkanen, Nanoscale Res. Lett. **9**, 398 (2014).
[38] V. I. Chegel, V. K. Lytvyn, A. M. Lopatynskyi, P. E. Shepeliavyi, O. S. Lytvyn, and Yu. V. Goltvyanskyi, Semi. Phys. Quant. Electron. Optoelectron. **18**, 272 (2015).
[39] *Plasmonics: Theory, and Applications*, edited by T. V. Shahbazyan and M. I. Stockman (Springer Dordrecht, 2013).
[40] J. Martorell, R. Vilaseca, and R. Corbalan, Phys. Rev. A **55**, 4520 (1997).
[41] J. Mäkitalo, S. Suuriniemi, and M. Kauranen, Opt. Express **19**, 23386 (2011); **21**, 10205 (2013).
[42] J. Dadap, J. Shan, and T. Heinz, J. Opt. Soc. Am. B **21**, 1328 (2004).
[43] J. E. Sipe and R. W. Boyd, Phys. Rev. A **46**, 1614 (1992).
[44] R. J. Gehr, G. L. Fischer, R. W. Boyd, and J. E. Sipe, Phys. Rev. A **53**, 2792 (1996).
[45] K. Dolgaleva and R. W. Boyd, Adv. Opt. Photonics **4**, 1 (2012).
[46] D. D. Smith, G. Fischer, R. W. Boyd, and D. A. Gregory, J. Opt. Soc. Am. B **14**, 1625 (1997).
[47] G. Piredda, D. D. Smith, B. Wendling, and R. W. Boyd, J. Opt. Soc. Am. B **25**, 945 (2008).
[48] L. A. Gomez, C. B. de Araujo, A. M. Brito-Silva, and A. Galembeck, Appl. Phys. B **92**, 61 (2008).
[49] R. F. Souza, M. A. R. C. Alencar, E. C. da Silva, M. R. Meneghetti, and J. M. Hickmann, Appl. Phys. Lett. **92**, 201902 (2008).
[50] H. B. de Aguiar, P. Gasecka, and S. Brasselet, Opt. Express **23**, 8960 (2015).